Effect of ZrO_2 interfacial layer on forming ferroelectric $Hf_xZr_yO_z$ on Si substrate

Cite as: AIP Advances **9**, 125020 (2019); https://doi.org/10.1063/1.5124402
Submitted: 14 August 2019 . Accepted: 19 November 2019 . Published Online: 17 December 2019

Sang Jae Lee, Min Ju Kim, Tae Yoon Lee, Tae In Lee, Jae Hoon Bong, Sung Won Shin, Seong Ho Kim, Wan Sik Hwang, and Byung Jin Cho

Effect of ZrO_2 interfacial layer on forming ferroelectric $Hf_xZr_yO_z$ on Si substrate

Cite as: AIP Advances 9, 125020 (2019); doi: 10.1063/1.5124402
Submitted: 14 August 2019 • Accepted: 19 November 2019 •
Published Online: 17 December 2019

Sang Jae Lee,[1] Min Ju Kim,[1] Tae Yoon Lee,[1] Tae In Lee,[1] Jae Hoon Bong,[1] Sung Won Shin,[1] Seong Ho Kim,[1] Wan Sik Hwang,[2] and Byung Jin Cho[1,a)]

AFFILIATIONS

[1] Department of Electrical Engineering, Korea Advanced Institute of Science and Technology, Daejeon 34141, South Korea
[2] Department of Material Engineering, Korea Aerospace University, Gyeonggi-do 10540, South Korea

[a)] Author to whom correspondence should be addressed: bjcho@kaist.edu

ABSTRACT

Ferroelectric $Hf_xZr_yO_z$ (HZO) with an average polarization switching window of 32 $\mu C/cm^2$ was demonstrated on a Si substrate with a ZrO_2 interfacial layer (IL). It is suggested that the ZrO_2 IL below HZO crystallizes in the form of an o-phase prior to HZO crystallization, during rapid thermal annealing, thereby promoting the vertical growth of an o-phase HZO layer. HZO with the ZrO_2 IL consists mainly of an o-phase that exhibits an in-plane tensile stress of 2.68 GPa, resulting in superior ferroelectric characteristics. This technology has the potential to expedite the realization of ferroelectric Hf-based dielectrics in advanced memory and logic technology.

Since the discovery of ferroelectricity in HfO_2, there has been great interest in both the fundamental science and the relevant device applications.[1–10] Of note, ferroelectric HfO_2 is emerging to have the greatest potential in both memory and logic devices.[7–10] While various approaches are being taken to enhance ferroelectricity in HfO_2 via different deposition techniques, different dopants and percentages, and different capping methods, most of the studies on ferroelectric HfO_2 have been performed on top of a metallic bottom electrode (typically TiN).[1–5] Although the fundamental science of ferroelectricity in Hf-based dielectrics on TiN has provoked curiosity, a stack of Hf-based dielectrics on a metal electrode is not a conventional stack of interest. In fact, it limits its applications, especially to MOS devices. Realizing ferroelectric Hf-based dielectrics on a semiconductor substrate would be of great interest for device applications but remains a challenge, especially with a Si substrate.[6,11,12] Recently, it was reported that the ZrO_2 interfacial layer (IL) on the TiN plays an important role in the nucleation of $Hf_xZr_{1-x}O_2$ (HZO). A ZrO_2 IL consisting mainly of an o-phase will tend to promote the o-phase in the HZO, resulting in superior ferroelectric characteristics in the HZO, compared to other ILs.[13] Although previous studies have demonstrated the ability of the ZrO_2 IL to form enhanced ferroelectric characteristics in the HZO, the HfO_2/ZrO_2/TiN stack is still not compatible with memory and logic devices and thus cannot be integrated in conventional processes.[13]

For the present study, we have successfully formed ferroelectric HZO on a Si substrate using a ZrO_2 IL. The HZO in the stack of the HZO/ZrO_2/Si substrate showed enhanced ferroelectricity, similar to the HZO in the stack of the HZO/ZrO_2/TiN electrode.[13] It was found that the ZrO_2 IL consisting mainly of the o-phase effectively exerted in-plane tensile stress in the HZO during crystallization, resulting in a stable o-phase and thereby, the ferroelectric HZO. A residual stress analysis conducted via the $\sin^2\Psi$ method using XRD indicated that with the ZrO_2 IL, the HZO was under tensile stress. These results have the potential to expedite the realization of ferroelectric HZO in advanced memory and logic technology.

First, a 2-nm thick ZrO_2 IL was deposited on a heavily doped p + Si (100) substrate after the conventional Si substrate cleaning process with H_2O_2:H_2SO_4 = 1:1 and the HF-last process. For comparison purposes, a sample with an Al_2O_3 IL was also prepared. Both the ZrO_2 and the Al_2O_3 ILs were deposited via atomic layer deposition (ALD) using tetrakis-ethyl-methyl-amino zirconium (TEMAZr) with ozone as a reactant gas at 300 °C and trimethyl-aluminium (TMA) with H_2O as a reactant gas at 200 °C,

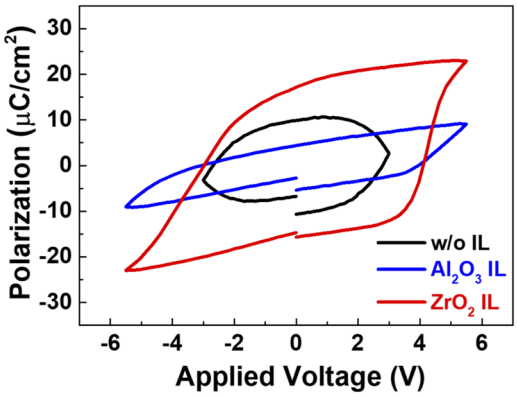

FIG. 1. P-V hysteresis of metal-ferroelectric-interlayer-Si capacitors with different interlayer dielectrics: without an additional interlayer (w/o IL), with a ~2 nm Al_2O_3 interlayer (Al_2O_3 IL), and with a ~2 nm ZrO_2 interlayer (ZrO2 IL). P-V measurements were conducted at 1 kHz.

respectively. A 9.5-nm thick HZO film with an Hf:Zr ratio of 0.87:0.13 was subsequently deposited on top of these ILs via radio-frequency (RF) cosputtering using HfO_2 and ZrO_2 targets. Next, a 40-nm thick TiN electrode was deposited on top of these HZO films via DC sputtering followed by rapid thermal annealing (RTA) in N_2 ambient at 900 °C for 1 min. After the crystallization of the HZO through the RTA process, Al was deposited via sputtering. Finally, the metal electrode was defined via conventional lithography and the dry etching process. The thicknesses of the dielectrics and the entire stack were measured using spectroscopic ellipsometry and a Cs-corrected scanning transmission electron microscope (STEM), respectively. A grazing incidence X-ray diffraction analysis (GIXRD) was conducted via the $\sin^2\varphi$ method at an incident angle of 0.5° to investigate the crystal structure of the film, which revealed residual stress in the HZO. Polarization-voltage (P-V) hysteresis curves and electrical properties were measured using a ferroelectric tester and parameter analyzer, respectively.

Figure 1 shows the typical P-V hysteresis curves of the HZO films with the ZrO_2 IL and Al_2O_3 IL, as well as without the IL between the HZO and Si substrate. The hysteresis loops of HZO with both the Al_2O_3 IL and ZrO_2 IL were measured in the range from −5.5 to 5.5 V, while those without the IL were measured in the range from −3 to 3 V due to the relatively high gate leakage current (data is not shown).

P-V curves caused by ferroelectricity were clearly observed from the HZO with both the Al_2O_3 IL and ZrO_2 IL. On the other hand, the HZO without the IL exhibited poor ferroelectricity due to the relatively high gate leakage current due to crystallized dielectrics with ultrathin equivalent oxide thickness (EOT).

The average polarization switching (P_{sw}: $P_r^+ - P_r^-$) value from the HZO with the ZrO_2 IL was 32 $\mu C/cm^2$, which outperformed the HZO without the IL and with the Al_2O_3 IL. This indicated that the ZrO_2 IL plays an important role in forming the low-EOT ferroelectric HZO dielectrics. In addition, the HZO with the ZrO_2 IL showed excellent uniformity (a standard deviation of 0.26 with a sample size of 25), which was attributed to the CMOS compatible process integration performed in this work.

To investigate the effect of the ZrO_2 IL on the ferroelectric properties of the HZO dielectrics on the Si substrate, the crystal structure and residual stress of the HZO with the ZrO_2 IL were compared with the HZO with the Al_2O_3 IL and without the IL using GIXRD. Figure 2(a) shows the GIXRD pattern of the HZO with the ZrO_2 IL and Al_2O_3 IL as well as without the IL. The broad diffraction peak in the range of 30°–32° arose from the (111) planes of the o-phase and monoclinic phase (m-phase) as well as the (011) plane of the tetragonal phase (t-phase). Their structural similarity created proximity between the peaks so that clear discrimination was challenging. Nevertheless, the diffraction peak near 36°, representing the (200) plane of the o-phase, was clearly observed only in the HZO with the ZrO_2 IL.

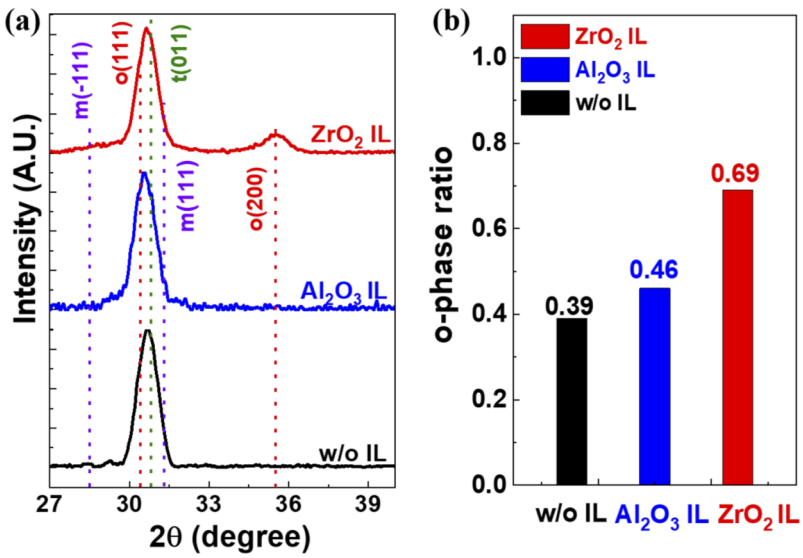

FIG. 2. (a) Grazing angle incidence X-ray diffraction (GIXRD) patterns of HZO capacitors with different interlayer dielectrics, (b) the relative ratio of the orthorhombic phase (o-phase/{(t-phase) + (m-phase)}) with different interlayer dielectrics.

Based on the results in Fig. 2(a), the relative ratio of the peak heights of the o-phase over the sum of both the t-phase and m-phase are presented in Fig. 2(b). This shows that the o-phase ratio in the HZO with the ZrO_2 IL was almost double that of the corresponding ratio without the IL. The above results adequately matched previous reports in which the t-phase to m-phase transition was suppressed, and the transformation to the o-phase was promoted when large in-plane tensile stress was applied to the HfO_2.[4–6] The formation of a noncentrosymmetric o-phase in the HfO_2 was a response to the ferroelectric properties in the HfO_2-based dielectrics.

To further quantify the stress exerted on the HZO with the addition of the IL, the stress value of the film was analyzed via the $\sin^2\varphi$ method using XRD. The stress value was obtained from the slope of the linear regression line using the least squares method on a $\sin^2\varphi$ (x-axis) − 2θ (y-axis) graph, as shown in the following equation:[14]

$$\sigma = K \cdot M = \left(-\frac{E}{2(1+\nu)} \cdot \cot\theta_0 \cdot \frac{\pi}{180}\right) \cdot \left(\frac{\Delta 2\theta}{\Delta \sin^2\varphi}\right), \quad (1)$$

where K, M, θ, E, ν, and φ represent the residual stress, stress constant, respective slope of the linear regression line, Young's modulus, Poisson's ratio, and the angle between the surface normal and lattice plane normal vectors, respectively. Based on Eq. (1), a graph of the 2θ function vs $|\sin^2\varphi|$ was plotted for the HZO with both the Al_2O_3 and ZrO_2 ILs as well as without the IL, as shown in Fig. 3.

The HZO with the ZrO_2 IL showed an excellent linearity factor of 0.95, and the respective stress was calculated to be 2.68 GPa (tensile stress value), which was sufficient to form an o-phase in the HfO_2 dielectrics.[15,16] Compared to the HZO with the ZrO_2 IL, the HZO with the Al_2O_3 IL exhibited a lack of linearity (a linearity factor of 0.61), as shown in Fig. 3(b), and the HZO without the IL [Fig. 3(a)] showed an oscillatory behavior, indicating inhomogeneous stress in the film. This residual stress analysis suggests that the ZrO_2 IL effectively induced more mechanical stress in the HZO than the Al_2O_3 IL, promoting the noncentrosymmetric o-phase in the HZO. The large amount of residual tensile stress in the metal/HZO/ZrO_2/Si stack originated, in part, from the relatively large thermal expansion coefficient (CTE) difference between the ZrO_2 (6.3×10^{-6} K) and Si substrate (3.08×10^{-6} K) compared with that between the Al_2O_3 (3.84×10^{-6} K) and Si substrate (3.08×10^{-6} K).[17–19] The ZrO_2 IL presumably crystallized in the form of the o-phase prior to HZO crystallization during the rapid thermal annealing process because the former had a lower crystallization temperature than the latter,[20,21] which is well supported by the following TEM analysis. Furthermore, the ZrO_2 plays a role as a capping layer to prevent the thermal stress release of the HZO layer.[22]

Figures 4(a) and 4(b) show the cross-sectional TEM images of the TiN/HZO/Si substrate and TiN/HZO/ZrO_2 IL/Si substrate, respectively. The average lattice fringe distance of the ZrO_2 IL shown in Fig. 4(b) was measured to be 2.9 Å, which was indexed to the (111) plane of the o-phase.[23] In this TEM image, an IL between the ZrO_2 IL and HZO layer is not distinguishable, which suggests that the o-phase ZrO_2 IL promoted the vertical growth of the o-phase HZO. In contrast, the TEM image of the HZO without the IL illustrated in Fig. 4(a) showed a mixture of different grains (different directions and different areas) and, in part, a hazy image. These TEM images clearly indicate that even the ultrathin ZrO_2 IL effectively promoted the noncentrosymmetric o-phase in the HZO via the induction of mechanical stress, resulting in the formation of ferroelectric HZO.

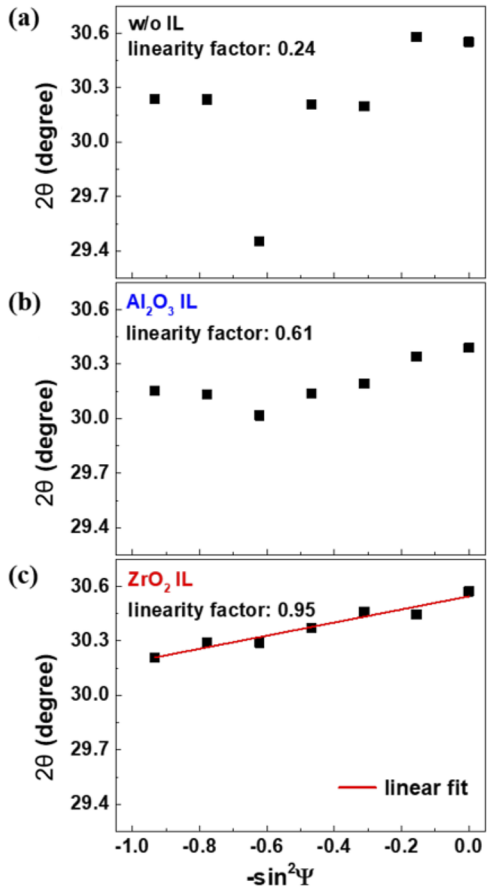

FIG 3. $-\sin^2\varphi$ vs 2θ plot of metal-ferroelectric-interlayer-Si capacitors with different interlayer dielectrics: (a) without additional IL, (b) with 2 nm Al_2O_3 IL, and (c) with 2 nm ZrO_2 IL.

It is worth mentioning that while preparing this manuscript, a similar approach with a ZrO_2 seed layer used to form a ferroelectric Hf-based dielectric was published.[24] We focused more on the stress analysis related to the ZrO_2 IL in the HZO, while the recent work focused more on device performance, particularly for next generation memory device applications.

Ferroelectric $Hf_{0.87}Zr_{0.13}O_2$ (HZO) was realized on a Si substrate with a 2-nm thick ZrO_2 IL between the HZO and Si substrate. Comparisons were also carried out with a HZO/Al_2O_3 IL/Si substrate and HZO/Si substrate. The HZO with the ZrO_2 IL exhibited robust ferroelectricity (showing a P_{sw} of 32 $\mu C/cm^2$) compared to those with the Al_2O_3 IL and without the IL. The experimental results revealed that the o-phase ZrO_2 IL induced in-plane tensile stress with a value of 2.68 GPa in the HZO, promoting the vertical growth of a noncentrosymmetric o-phase in the HZO during the crystallization annealing process. This stack technology, leveraging the ferroelectric HZO on a Si substrate with a ZrO_2 IL, can expedite the exploitation of ferroelectricity in advanced memory and logic devices.

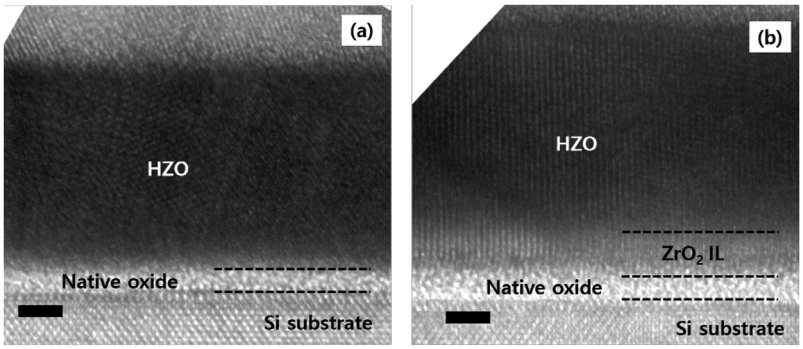

FIG 4. Cross-sectional TEM image (a) without additional interlayer (w/o IL) and (b) with ZrO_2 interlayer (ZrO_2 IL).

This work was supported by the Center for Advanced Soft-Electronics, which is funded by the Ministry of Science, ICT and Future Planning, through the Global Frontier Project (Grant No. CASE-2011-0031638).

REFERENCES

[1]T. S. Böscke, J. Müller, D. Bräuhaus, U. Schröder, and U. Böttger, Appl. Phys. Lett. **99**(10), 102903 (2011).
[2]J. Müller, T. S. Böscke, U. Schröder, S. Mueller, D. Bräuhaus, U. Böttger, L. Frey, and T. Mikolajick, Nano Lett. **12**(8), 4318–4323 (2012).
[3]L. Xu, T. Nishimura, S. Shibayama, T. Yajima, S. Migita, and A. Toriumi, J. Appl. Phys. **122**(20), 124104 (2017).
[4]M. H. Park, H. J. Kim, Y. J. Kim, T. Moon, and C. S. Hwang, Appl. Phys. Lett. **104**(7), 072901 (2014).
[5]M. H. Park, H. J. Kim, Y. J. Kim, W. Lee, T. Moon, K. D. Kim, and C. S. Hwang, Appl. Phys. Lett. **105**(7), 072902 (2014).
[6]T. Shiraishi, K. Katayama, T. Yokouchi, T. Shimizu, T. Oikawa, O. Sakata, H. Uchida, Y. Imai, T. Kiguchi, T. J. Konno, and H. Funakubo, Appl. Phys. Lett. **108**(26), 262904 (2016).
[7]A. Aziz, E. T. Breyer, A. Chen, X. Chen, S. Datta, S. K. Gupta, M. Hoffmann, X. S. Hu, A. Ionescu, M. Jerry, T. Mikolajick, H. Mulaosmanovic, K. Ni, M. Niemier, I. O'Connor, A. Saha, S. Slesazeck, S. K. Thirumalal, and X. Yin, in *2018 Design, Automation and Test in Europe Conference and Exhibition* (IEEE, 2018), pp. 1289–1298.
[8]M. Jerry, P.-Y. Chen, J. Zhang, P. Sharma, K. Ni, S. Yu, and S. Datta, in *IEEE International Electron Devices Meeting* (IEEE, 2017), pp. 6.2.1–6.2.4.
[9]T. Ali, P. Polakowski, S. Riedel, T. Büttner, T. Kämpfe, M. Rudolph, B. Pätzold, K. Seidel, D. Löhr, R. Hoffmann, M. Czernohorsky, K. Kühnel, P. Steinke, J. Calvo, K. Zimmermann, and J. Müller, IEEE Trans. Electron Devices **65**(9), 3769–3774 (2018).
[10]S. Salahuddin and S. Datta, Nano Lett. **8**(2), 405–410 (2007).
[11]P. D. Lomenzo, Q. Takmeel, C. M. Fancher, C. Zhou, N. G. Rudawski, S. Moghaddam, J. L. Jones, and T. Nishida, IEEE Electron Device Lett. **36**(8), 766–768 (2015).
[12]Y. Goh and S. Jeon, Nanotechnology **29**(33), 335201 (2018).
[13]T. Onaya, T. Nabatame, N. Sawamoto, and A. Ohi, Appl. Phys. Express **10**(8), 081501 (2017).
[14]M. E. Fitzpatrick, A. T. Fry, P. Holdway, F. A. Kandil, J. Shackleton, and L. Suominen, *National Physical Laboratory Measurement Good Practice Guide* (NPL, 2005), pp. 1–68.
[15]J. E. Lowther, J. K. Dewhurst, J. M. Leger, and J. Haines, Phys. Rev. B **60**(21), 14485 (1999).
[16]E. H. Kisi, J. Am. Ceram. Soc. **81**(3), 741–745 (1998).
[17]T. Schenk, S. M. Fancher, M. H. Park, C. Richter, C. Künneth, A. Kersch, J. L. Jones, T. Mikolajick, and U. Schroeder, Adv. Electron. Mater. **5**, 1990303 (2019).
[18]M. Cassir, F. Goubin, C. Bernay, P. Vernoux, and D. Lincot, Appl. Surf. Sci. **193**(1), 120–128 (2002).
[19]M. Berdova, "Micromechanical characterization of ALD thin films," Ph.D. thesis, Aalto University, 2015.
[20]S. V. Ushakov, A. Navrotsky, Y. Yang, S. Stemmer, K. Kukli, M. Ritala, M. A. Leskelä, P. Fejes, A. Demkov, C. Wang, B. Y. Nguyen, D. Triyoso, and P. Tobin, Phys. Status Solidi B **241**(10), 2268–2278 (2004).
[21]M. H. Park, H. J. Kim, Y. J. Kim, W. Lee, T. Moon, and C. S. Hwang, Appl. Phys. Lett. **102**(24), 242905 (2013).
[22]Y. W. Lu, J. Shieh, and F. Y. Tsai, Acta Mater. **115**(15), 68–75 (2016).
[23]H. J. Kim, M. H. Park, Y. J. Kim, Y. H. Lee, W. Jeon, T. Gwon, T. Moon, K. D. Kim, and C. S. Hwang, Appl. Phys. Lett. **105**(19), 192903 (2014).
[24]W. Xiao, C. Liu, Y. Peng, S. Zheng, Q. Feng, C. Zhang, J. Zhang, Y. Hao, M. Liao, and Y. Zhou, IEEE Electron Device Lett. **40**(5), 714–717 (2019).